Defect-induced hyper-Raman spectra in cubic zirconia

S. Shin and M. Ishigame
Research Institute for Scientific Measurements, Tohoku University, 2-1-1 Katahira, Sendai, Miyagi 980, Japan
(Received 21 July 1986)

Hyper-Raman scattering of cubic zirconia and CaF_2 is measured at room temperature. For a CaF_2 crystal, the frequencies of the TO and LO modes with T_{1u} symmetry are determined to be 260 and 480 cm^{-1}, which are in good accord with the results of infrared measurements. In a fluorite-type cubic zirconia, the defect-induced hyper-Raman spectra due to the oxygen vacancies are observed. The structures of the hyper-Raman spectra are reasonably explained by the frequency distribution of hyper-Raman-active modes in the whole Brillouin zone, which is estimated from the imaginary part of the simple projections of the phonon displacement-displacement Green's functions onto a defect space consisting of an O_6 molecule. From the analysis of the mode vectors for the O_6 molecule, the attempt frequency of oxygen ions is found to correspond to the 690-cm^{-1} band in the observed hyper-Raman spectra with T_{1u} symmetry.

I. INTRODUCTION

Cubic zirconia is a well-known superionic conductor of oxygen ions, from which many applications are derived. In basic studies of superionic conductors, cubic zirconia is also one of the most noticeable materials, because it has a simple crystal structure in the superionic conductor in which it is easy to see the ion hopping process.

The crystal structure of cubic zirconia stabilized with Y_2O_3 is a disordered CaF_2-type structure [O_h^5 ($Fm3m$)]. Zr^{4+} ions are randomly replaced by Y^{3+} ions in cubic zirconia, and consequently there are many oxygen vacancies which keep the charge neutrality. The O^{2-} ions begin to hop toward these vacancies at high temperatures. In the simple hopping process with a thermal activation energy, it is well known that the conductivity can be determined by the two quantities, an activation energy Δ and an attempt frequency ν. The activation energy is determined by the barrier height between the potential wells. The attempt frequency is a vibrational frequency of the ion involved in the hopping. Thus, the hopping rate Γ is written as $\Gamma=\sum_\lambda \nu_\lambda e^{-\Delta_\lambda/kT}$, where λ indicates the kind of hopping channel for hopping ions. Then, the activation energy and the attempt frequency values have been obtained from the measurements of conductivities,[1-7] NMR, γ-γ angular correlation,[8] and quasielastic light scattering,[9-12] so far. However, in these measurements, the attempt frequency is a fitting parameter, while the activation energy is obtained directly. The most conventional experimental technique to determine the attempt frequency is Raman scattering or infrared absorption measurements, where the attempt frequency is shown as the structure in the spectra.[13] However, it is generally rather difficult to determine the attempt frequency from the spectra, because the assignment of the spectra is not easy to determine without information about the concrete motion of the hopping ions.

In the case of cubic zirconia, the attempt frequency has not been found by means of Raman scattering[14,15] and infrared absorption.[16] In Raman spectra of this material,[14,15] very curious and diffusive structures are found in each polarization of A_g, E_g, and T_{2g}, while the first-order Raman-active mode is only T_{2g} at the Γ point in the Brillouin zone for the fluorite structure. On the contrary, in the case of infrared spectra,[16] well-defined LO and TO modes have been found experimentally with rather broad linewidths.

Recently, hyper-Raman scattering has been found to be a useful technique for the study of lattice vibrations,[17] since the selection rules of hyper-Raman scattering are quite different from those of Raman scattering. From the selection rules, the infrared-active mode as well as the silent mode are included in hyper-Raman scattering. In this paper we first measure the hyper-Raman scattering of the CaF_2 single crystal to get the typical hyper-Raman spectra of the CaF_2-type perfect crystal. Next, we measure the hyper-Raman spectra of cubic zirconia. The purpose of this paper is to obtain information about the motion of hopping ions through the defect-induced hyper-Raman spectra, which in turn will indicate the attempt frequency of hopping ions in cubic zirconia.

II. EXPERIMENT

An acoustic Q-switched Nd-YAG (yttrium-aluminum-garnet) laser of wavelength 1.06 μm was used as a source of excited radiation. The peak power of pulses was 20 kW at 1 kHz. The polarized laser beam with a single mode was focused on the samples using a lens of $f=100$ mm. All measurements were done at room temperature. The hyper-Raman scattering light at right angles to the incident light was focused through a condenser lens after passing through an analyzer. A single monochromator of $F=4.2$ was used with a resolution of about 50 cm^{-1} which corresponds to a slit width of 0.5 mm. Since the intensity of the hyper-Raman scattering light was very low, a gated photon counter system was used to reduce the dark levels of the photomultiplier by about 1/10000. The

unpolarized light was used for hyper-Raman scattering of CaF_2 crystals because the hyper-Raman scattering intensity of this material is extremely weak.

The single crystals of CaF_2 were made by the Harshaw Chemical Company. The single crystals of cubic zirconia $(ZrO_2)_{1-x}$ $(YO_{1.5})_x$ with $x=0.18$ were made by the skull-melting method[18] at the Lebedov Physical Institute of Academia Naukaite, USSR. The single crystal was cut into a cube with faces parallel to (100) with the dimensions $10\times5\times5$ mm^3 and polished. Polycrystals of $x=0.23$, 0.18, 0.15, and 0.13 were made by the floating-zone method using a xenon-arc image furnace in our institute. The polycrystals of cubic zirconia of $x=0.67$ and 0.33 were grown from a melt by using the 10-m solar furnace at our Institute.[19] The structure of these crystals was confirmed to be a fluorite-type crystal using x-ray diffraction analysis.

III. RESULTS

A. Hyper-Raman spectra of CaF_2 crystal

The crystal structure of CaF_2 consists of three interpenetrating face-centered-cubic lattices and belongs to the space group O_h^5. The factor group analysis using point group O_h indicates that there are two optic modes T_{2g} and T_{1u} at the Γ point in the Brillouin zone. From the selection rules for hyper-Raman tensors of the CaF_2 crystal, only the T_{1u} mode is active for hyper-Raman scattering. It is well known that the long-wavelength T_{1u} optic mode splits into LO and TO modes in a macroscopic electric field. Therefore, two hyper-Raman bands of the LO and TO modes are expected to appear in the hyper-Raman spectra.

Figure 1 is a hyper-Raman spectrum of a CaF_2 single crystal. In this figure, the second-harmonic-generation (SHG) radiation centered at a 0-cm^{-1} shift has little intensity, though the SHG is forbidden by the centrosymmetric structure of the CaF_2 crystal. The origin of SHG radiation for CaF_2 crystals may come from the impurities in the crystals, as are seen in other ionic crystals.[20–22] Two hyper-Raman bands at 260 and 480 cm^{-1} are clearly observed. Furthermore, a weak shoulder at the low-frequency-side tail of the 480-cm^{-1} band is also observed around 400 cm^{-1} in this spectrum. When compared to infrared measurements,[23] distinct hyper-Raman bands of 260 and 480 cm^{-1} can be assigned undoubtedly to the TO and LO modes, respectively. In this measurement, the linewidth of SHG is comparable to those of the LO and TO modes without deconvolution by a slit function. To get the correct line shape of a spectrum, the spectrum should be deconvoluted by a slit function. However, since the slit width of the monochromator was widened due to the low intensity of scattered light, the correct line shape could not be determined.

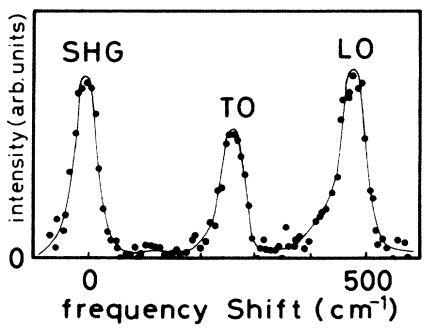

FIG. 1. Hyper-Raman spectrum of CaF_2 at room temperature.

It is interesting to compare the hyper-Raman spectra with the conductivity spectra of the CaF_2 crystal which are obtained by infrared measurements, because the CaF_2 crystal has the conductivity due to the density of combined vibrational states in the frequency region between ω_{TO} and ω_{LO}. Infrared absorption due to the density of combined vibrational states has already been observed.[23] In hyper-Raman spectra, the similar structures are observed around 400 cm^{-1}.

From the results obtained above, it is found for CaF_2 crystal that the hyper-Raman spectra give information about the infrared-active phonons, including the multiphonon process.

B. Hyper-Raman spectra of cubic zirconia

Figure 2 shows the hyper-Raman spectra of cubic zirconia. Closed circles are the depolarized spectrum $[X(ZX)Y]$ and open circles are the polarized spectrum $[X(ZZ)Y]$, where an orthogonal Cartesian coordinate X,Y,Z is chosen parallel to the crystal axis [100]. In this figure, a distinct hyper-Raman band is observed clearly at 690 cm^{-1}. However, in contrast to the hyper-Raman spectra of the CaF_2 crystal, a broad band with many structures is observed in a frequency region below 400 cm^{-1}. The SHG spectrum is also observed at 0 cm^{-1} with a rather strong intensity. The gross features of the

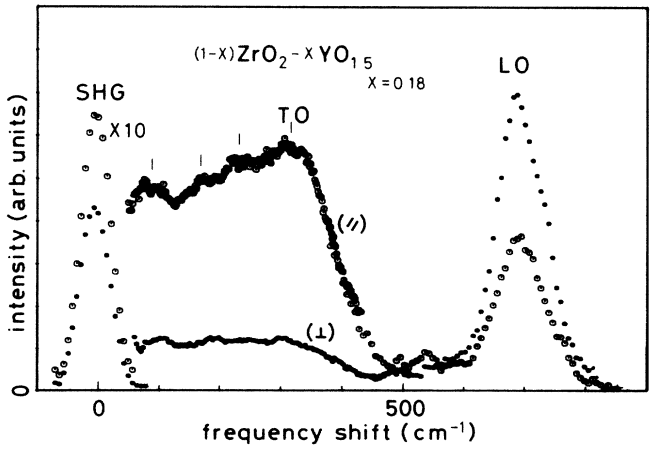

FIG. 2. Polarized hyper-Raman spectra of cubic zirconia $(ZrO_2)_{1-x}(YO_{1.5})_x$ with $x=0.18$ at room temperature. Open circles are the polarized spectrum (//)and closed circles are the depolarized spectrum (⊥).

two polarized spectra are similar to each other. However, the intensity ratio of the polarized and the depolarized spectra in each structure is very different. The intensity of the polarized spectrum is stronger than that of the depolarized spectrum in the frequency range below 400 cm^{-1}. The intensity of SHG in the polarized spectrum is also stronger than that of the depolarized one by a factor of 1.5. On the other hand, for the band at 690 cm^{-1}, the intensity of the depolarized spectrum is stronger than that of the polarized one. From these measurements, it is found that the hyper-Raman spectra of cubic zirconia are very different from those of CaF_2 on three points: (i) The spectra of cubic zirconia have a number of structures. Especially in the low-frequency range, many structures are observed in contrast to the spectra of CaF_2. (ii) The spectral structures are diffusive, differing from those of CaF_2. (iii) The intensity of SHG in cubic zirconia is stronger than that in CaF_2.

These curious features of the spectra of cubic zirconia seem to be, of course, due to the crystal structure which has many vacancies in oxygen-ion sublattices and Y^{3+} ions in a Zr^{4+}-ion sublattice. That is, the destruction of the translational symmetry of the crystal leads to the relaxation of the $k=0$ selection rule in light scattering so that all phonons in the Brillouin zone will become active in the case of the hyper-Raman effect in cubic zirconia. The SHG can also be allowed, because of the breakdown of centrosymmetry at the defects.

Figure 3 shows the hyper-Raman spectra of cubic zirconia with the various composition of Y^{3+} ions in the frequency range of 0–500 cm^{-1}. In this figure, the intensity of the spectrum is normalized to match the intensity of the band at 690 cm^{-1} to equal each other, since the intensity of this band does not vary much with the Y^{3+}-ion composition. From this figure, it is found that the frequency of each peak does not vary with the value of x. However, there is a distinct variation of the intensity of the spectra on the low-frequency side of 316 cm^{-1}, as compared to the intensity at the peak of 316 cm^{-1}. As is seen from Fig. 3, the intensity of the low-frequency-side spectra decreases as the concentration of Y^{3+} ions (or oxygen vacancies) increases. This fact suggests that the hyper-Raman spectra observed in cubic zirconia may include the defect-induced hyper-Raman spectra.

It is worthwhile to compare the hyper-Raman spectra with the infrared absorption spectrum,[16] because these two measurements have similar selection rules. Figure 4 shows both spectra. Polarized hyper-Raman spectra (dots) are reduced by the Bose-Einstein factor to eliminate the temperature effects. The dashed curve is the infrared absorption spectrum obtained at normal incidence by using thin film. The dotted curve is the absorption spectrum at oblique incidence (55°). In the comparison of hyper-Raman spectra with infrared spectra, one can see that the structure of hyper-Raman spectra observed at around 316 cm^{-1} is a TO-like band, and at around 690 cm^{-1} it is a LO-like band. The infrared and the hyper-Raman spectra are very similar in gross features. This

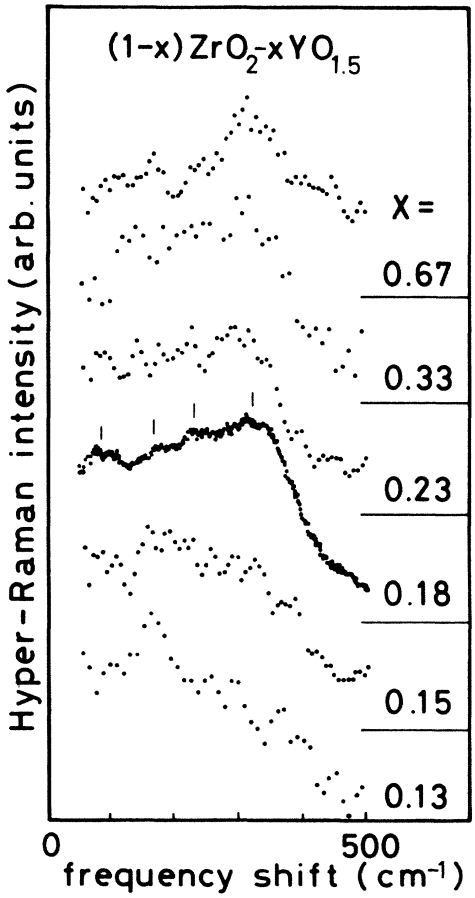

FIG. 3. x dependence of hyper-Raman spectra of cubic zirconia $(ZrO_2)_{1-x}(YO_{1.5})_x$. $x=0.67$, 0.33, 0.23, 0.18, 0.15, and 0.13.

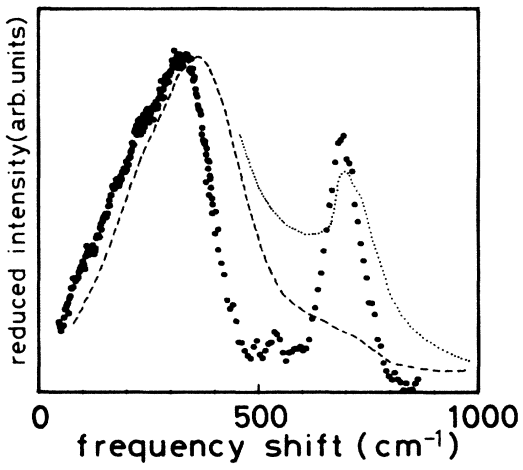

FIG. 4. Closed circles show the hyper-Raman spectrum of $(ZrO_2)_{1-x}(YO_{1.5})_x$ with $x=0.18$ at 300 K reduced by using the Bose-Einstein factor. The dashed curve is the absorption spectrum of thin film of cubic zirconia ($x=0.18$) at normal incidence. The dotted curve is the absorption spectrum of the same thin film at oblique incidence.

fact implies that both spectra reflect the frequency distribution of phonons in the Brillouin zone which become active in hyper-Raman or infrared absorption by the defects. The similarity of the two spectra may be due to the very similar selection rules. However, we can see many structures below 316 cm^{-1} in hyper-Raman spectra measured at 300 K, as seen in Fig. 2. Structures in this frequency region, however, cannot be seen clearly in the reduced hyper-Raman spectra or in the infrared absorption spectra measured at 300 K. This is the remarkable point of the hyper-Raman effect because the scattering intensity of the hyper-Raman effect depends heavily on the temperature through the Bose-Einstein factor for low-energy excitation. However, the intensity of the infrared absorption is almost independent of temperature.

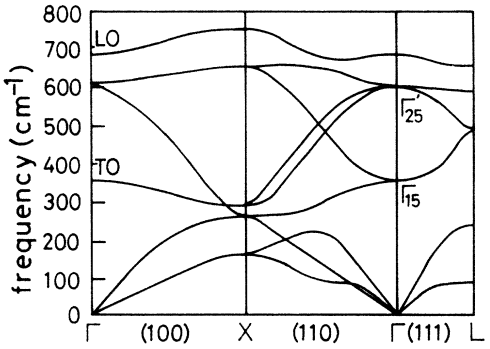

FIG. 5. Calculated phonon dispersion curves of cubic zirconia by using the rigid-ion model for the virtual ion crystal.

IV. DISCUSSION

A. Defect-induced spectra

In order to reveal the structures of the defect-induced hyper-Raman spectra, it is necessary to know the lattice vibrational properties of cubic zirconia. However, in cubic zirconia, the cation sublattice consists of Zr^{4+} and Y^{3+} ions, and the anion sublattice consists of oxygen ions and vacancies. These modifications of each sublattice mean that values of force constants, effective charges, and ionic masses depend on each ion site. However, it is shown from infrared studies that the virtual-ion-crystal model can be applied to cubic zirconia, in which the crystal of cubic zirconia is assumed to be a perfect fluorite-type crystal consisting of ions with virtual mass, virtual charge, and virtual force constants, weighted by x. Then, we can calculate the dispersion curves using the ordinary method. The defect-induced hyper-Raman spectra can be calculated according to the theory of Lacina and Pershan.[24] A more detailed description will be given in another paper.[15]

For the $(ZrO_2)_{1-x}(YO_{1.5})_x$ crystal, the virtual masses M(cation) and M(anion) and the virtual charges e(cation) and e(anion) are assumed to be represented by the following equations, where M(Zr), M(Y), and M(O) are masses of Zr^{4+}, Y^{3+}, and O^{2-} ions, respectively, and e(Zr), e(Y), and e(O) are charges of each ion, respectively:

$$M(\text{cation})=(1-x)M(\text{Zr})+xM(\text{Y}) , \quad (1)$$

$$M(\text{anion})=(1-x/4)M(\text{O}) , \quad (2)$$

$$e(\text{cation})=(1-x)e(\text{Zr})+xe(\text{Y})=4Z_e , \quad (3)$$

$$e(\text{anion})=(1-x/4)e(\text{O})=2Z_e . \quad (4)$$

Virtual effective charge Z_e can be written as $Z_e=Z_O(1-x/4)$, where $Z_O=0.585$ is obtained from infrared measurements.[16] The six unknown virtual force constants can be estimated from the experimental values of C_{11}, C_{12}, C_{44}, ω_{TO}, ω_{LO}, and ω_R, shown in Table I. These elastic constants are measured by the hypersonic method, and ω_{TO} and ω_{LO} are obtained by infrared measurements. The value of ω_R is rather obscure since the observed Raman spectra[14,15] with the symmetry T_{2g} have many structures. So, we assumed that the value of ω_R is 605 cm^{-1}, which is the most distinct Raman peak obtained by the same cubic zirconia.

Figure 5 shows the calculated phonon dispersion curves along the high symmetric lines in the Brillouin zone which are reproduced from Ref. 15. It can be seen that the critical points of the dispersion curves show a considerably good correspondence to the structures of hyper-Raman spectra.

In order to carry out detailed calculations of defect-induced hyper-Raman spectra, the virtual defect space must be considered. Because the introduction of defects leads to the breakdown of the wave vector $k=0$ selection rule, phonons in all parts of the Brillouin zone will contribute to hyper-Raman spectra. In the case of cubic zirconia, we define the defect space as consisting of an oxygen vacancy and its nearest neighbor—six oxygen ions, as shown in Fig. 6. The reason why we use the defect space described above is as follows: (i) Two types of defects exist in this material. These are the vacancy at the oxygen-ion site and the Y^{3+} ion at the Zr^{4+}-ion site. However, the changes of mass and charge at the defect of the oxygen-ion site are larger than those at the defect of the

TABLE I. Experimental data on $(ZrO_2)_{1-x}(YO_{1.5})_x$ with $x=0.18$. C_{11}, C_{12}, and C_{44} are elastic constants. ω_R, ω_{TO}, and ω_{LO} are Raman, infrared resonance, and longitudinal optic frequencies, respectively.

C_{11} (10^{12} dyn/cm^2)	C_{12} (10^{12} dyn/cm^2)	C_{44} (10^{12} dyn/cm^2)	ω_R (cm^{-1})	ω_{TO} (cm^{-1})	ω_{LO} (cm^{-1})
3.75	0.75	0.64	605	354	680

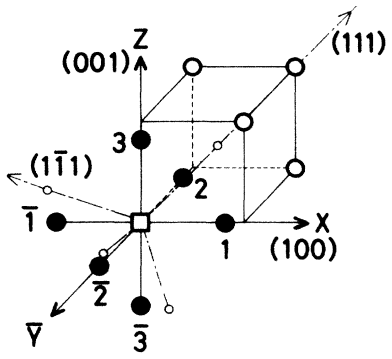

FIG. 6. A configuration of ions around a vacancy for the cubic zirconia. The square is an oxygen vacancy. The small open circles are metal ions. The large open circles are oxygen ions at normal positions. The closed circles are six oxygen ions displaced along the (100) directions toward the oxygen vacancy.

Zr^{4+}-ion site. Therefore, as a first approximation, we consider only the O^{2-} vacancy as the defect. (ii) The vacancy is surrounded octahedrally by six oxygen ions and tetrahedrally by four metal ions. By means of a neutron scattering experiment, the surrounding oxygen ions are found to be displaced toward the vacancy to a much greater degree than the surrounding four metal ions.[25] (iii) The most important reason is that we are interested in the motion of the oxygen ions beside the vacancy because these ions will be able to hop to the vacancy.

If we assume that the defect space consists of six oxygen ions ignoring the four metal ions, the symmetry of defect space will be O_h. Vibrational normal modes of this O_6 molecule can be given as $A_{1g}+E_g+T_{1g}+T_{2g}+2T_{1u}+T_{2u}$. The unnormalized mode vectors of an O_6 molecule are shown in Table II, which are reproduced from Ref. 15. In these modes, Raman-active modes are A_{1g}, E_g, and T_{2g}. The infrared-active mode is T_{1u}. Hyper-Raman-active modes are T_{1u} and T_{2u}, where T_{2u} is the silent mode. By using phonon displacement-displacement Green's functions $G(\omega+i\varepsilon)$ which are estimated by the phonon dispersion curves calculated by a virtual-ion-crystal model, we can estimate the frequency distribution of hyper-Raman-active modes in the whole Brillouin zone which is the imaginary part of the simple projections of the unperturbed Green's functions $G(\omega+i\varepsilon)$ onto the defect space. According to the theoretical treatment by Lacina and Pershan,[24] the defect-induced hyper-Raman spectra $I(\omega;T_{1u})$ and $I(\omega;T_{2u})$ can be represented by the following equations:

$$I(\omega;T_{1u})=\mathrm{Im}\langle T_{1u}\,|\,G(\omega+i\varepsilon)\,|\,T_{1u}\rangle\ , \tag{5}$$

$$I(\omega;T_{2u})=\mathrm{Im}\langle T_{2u}\,|\,G(\omega+i\varepsilon)\,|\,T_{2u}\rangle\ . \tag{6}$$

Here, $\langle T_{1u}|$ and $\langle T_{2u}|$ are the hyper-Raman-active mode vectors in an O_6 molecule which are given in Table II. The calculated results are shown by histograms in Fig. 7.

The T_{1u} mode which is given by the diagonal term of the hyper-Raman tensor[26] will appear in polarized spectra. Then, the frequency distributions of two calculated $T_{1u}(1)$ and $T_{1u}(2)$ modes must be added in order to com-

TABLE II. Unnormalized mode vectors for an O_6 molecule in the symmetry subspace given by the decomposition using the group analysis.

	A_{1g}	E_g		T_{1g}			T_{2g}			$T_{1u}(1)$			$T_{1u}(2)$			T_{2u}		
1	1	−2	0	0	0	0	0	0	0	1	0	0	−2	0	0	0	0	0
	0	0	0	0	0	1	0	0	1	0	1	0	0	1	0	0	1	0
	0	0	0	0	−1	0	0	1	0	0	0	1	0	0	1	0	0	−1
2	0	0	0	0	0	−1	0	0	1	1	0	0	1	0	0	−1	0	0
	1	1	−1	0	0	0	0	0	0	0	1	0	0	−2	0	0	0	0
	0	0	0	1	0	0	1	0	0	0	0	1	0	0	1	0	0	1
3	0	0	0	0	1	0	0	1	0	1	0	0	1	0	0	1	0	0
	0	0	0	−1	0	0	1	0	0	0	1	0	0	1	0	0	−1	0
	1	1	1	0	0	0	0	0	0	0	0	1	0	0	−2	0	0	0
$\bar{1}$	−1	2	0	0	0	0	0	0	0	1	0	0	−2	0	0	0	0	0
	0	0	0	0	0	−1	0	0	−1	0	1	0	0	1	0	0	1	0
	0	0	0	0	1	0	0	−1	0	0	0	1	0	0	1	0	0	−1
$\bar{2}$	0	0	0	0	0	1	0	0	−1	1	0	0	1	0	0	−1	0	0
	−1	−1	1	0	0	0	0	0	0	0	1	0	0	−2	0	0	0	0
	0	0	0	−1	0	0	−1	0	0	0	0	1	0	0	1	0	0	1
$\bar{3}$	0	0	0	0	−1	0	0	−1	0	1	0	0	1	0	0	1	0	0
	0	0	0	1	0	0	−1	0	0	0	1	0	0	1	0	0	−1	0
	−1	−1	−1	0	0	0	0	0	0	0	0	1	0	0	−2	0	0	0

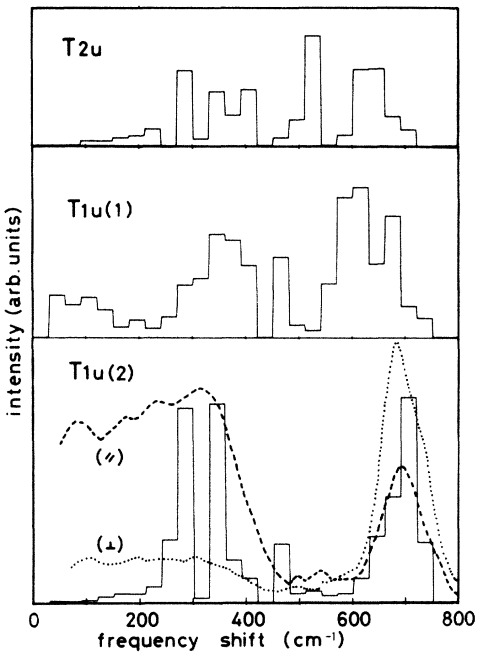

FIG. 7. Calculated frequency distributions of hyper-Raman-active modes induced by a defect. The dotted curve is the depolarized hyper-Raman spectra. The dashed curve is the polarized hyper-Raman spectra.

pare the calculated frequency distribution with the polarized hyper-Raman spectra. The gross feature of the experimental spectra can be elucidated by the calculated spectra. In the observed spectra, we can see five structures at 88, 170, 233, 316, and 690 cm^{-1}. The structure around 88 cm^{-1} will be derived from the acoustic branches which appear mainly in the frequency distribution of the $T_{1u}(1)$ mode. From the comparison of the hyper-Raman spectra with the phonon energy at critical points in the Brillouin zone, it is seen that the structure around 316 cm^{-1} mainly comes from the TO mode, and the isolated structure near 690 cm^{-1} mainly comes from the LO mode. However, for the perfect CaF_2-type crystal, the LO mode should be forbidden in polarized spectra in the case of this scattering configuration, because the hyper-Raman intensity $I(\omega)$ is given[27] by

$$I(\omega)=\sum | e_s^i e_0^j e_0^k d_{ijk}^{v(l)} \xi_l |^2 ,$$

where $d_{ijk}^{v(l)}$ is a hyper-Raman tensor. e_s and e_0 are the polarization vectors of the electric fields of scattered and incident light, respectively, and ξ is the polarization unit vector of the phonon. Each i,j,k and l is one of the axis of Cartesian coordinates X, Y, and Z. Since there exists a rather strong intensity of the hyper-Raman spectra corresponding to the phonon energy of the LO mode in polarized spectra, one can see that the band at 690 cm^{-1} mainly comes from the defect-induced spectra rather than from the pure LO mode.

On the other hand, depolarized spectra which are given by the off-diagonal terms of the hyper-Raman tensor, are the sum of the $T_{1u}(1)$, $T_{1u}(2)$, and T_{2u} modes. The frequency distribution of the T_{2u} mode does not have the distinct peak, as seen from Fig. 7, so that the structure of the depolarized spectra may be considered to reflect the frequency distribution of the $T_{1u}(1)+T_{1u}(2)$ modes rather than that of the T_{2u} mode.

There remain some discrepancies between the experimental and the calculated spectra. The distinct discrepancy is that the intensity of the calculated spectra is too weak compared with the intensity of the observed spectra in the frequency range from 170 to 233 cm^{-1}. As the phonons in this energy range correspond to those at the critical point X, it is thought that the model of defect space used here may be insufficient to estimate the frequency distribution contributed to these bands. It is interesting to see the correlation between the intensity of the bands from 170 to 233 cm^{-1} and the concentration of Y^{3+} ions (or oxygen vacancies). As seen from Fig. 3, the observed intensity of these bands has a tendency to increase with the decreasing of the concentration of Y^{3+} ions. According to the phase diagram,[28] the $(ZrO_2)_{1-x}(YO_{1.5})_x$ crystal is "impatient" to have the tetragonal symmetry in the low concentration of Y^{3+} ions. Therefore, there is a possibility of hyper-Raman scattering due to the lowering of symmetry of the crystal structure for the bands at 170 and 233 cm^{-1}. Another disadvantage for the defect space model used here is that only the six oxygen ions surrounding the vacancy are employed for the calculation of hyper-Raman spectra, ignoring the four metal ions which are surrounding each vacancy. Taking account of these four metal ions, the symmetry of defect space is lowered from O_h to T_d, assuming that the four metal ions are the same. This lowering of the symmetry of defect space may cause extra contributions to hyper-Raman spectra.

From these considerations, except for the discrepancy of the intensity between the calculated and the experimental spectra, the hyper-Raman spectra in cubic zirconia can be well explained by the defect-induced hyper-Raman scattering.

B. Attempt frequency

If we define the defect space which is composed of the six oxygen ions beside the vacancy, the mode vectors of A_{1g}, E_g, T_{1g}, T_{2g}, $2T_{1u}$, and T_{2u} can be assumed to make a complete set for the motion of these ions. The attempt frequency is thought to be the vibrational frequency of oxygen ions beside the vacancy, which should belong to one of the mode vectors, because one of these ions will be able to hop to the vacancy. Therefore, the attempt frequency must be included in the calculated defect-induced spectra. Even if we consider a larger defect space than that used here, the displacements of these six oxygen ions can be completely described by the linear combination of the A_{1g}, E_g, T_{1g}, T_{2g}, $2T_{1u}$, and T_{2u} mode vectors under the assumption mentioned above.

Now, we consider what kind of vibrational modes include the attempt frequency. First, it is clear that, in the mode which includes an attempt frequency, the mode vector should show the displacement of the oxygen ion to-

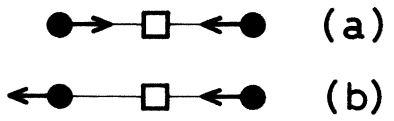

FIG. 8. Typical motion of oxygen ions beside the oxygen vacancy in Raman mode (a) and hyper-Raman mode (b).

ward the vacancy. Then, the candidates of the modes concerned with the attempt frequency are A_{1g}, E_g, $T_{1u}(1)$, and $T_{1u}(2)$ modes, as seen in Table II. In the case of gerade modes, however, the oxygen ions on both sides of the vacancy move toward the vacancy at the same time [Fig. 8(a)], so that both ions will move closer to each other. In this case, a strong Coulomb repulsive force exists between the two ions, which prevents the oxygen ion from hopping toward the vacancy. On the other hand, in the case of ungerade modes, oxygen ions on both sides of the vacancy move in the same direction in phase, keeping the same distance [Fig. 8(b)]. In this case, the Coulomb repulsive force acts as a propulsion of the oxygen ion hopping toward the vacancy. Thus, the motion of ungerade modes can assist the hopping of the oxygen ion to the vacancy. Therefore, we can expect that the attempt frequency will be included in the hyper-Raman spectra with T_{1u} symmetry. If the hopping rate Γ is assumed to be given by the equation $\Gamma=\sum_\lambda \nu_\lambda e^{-\Delta_\lambda/kT}$ using the attempt frequency ν_λ and the activation energy Δ_λ, the highest vibrational frequency of oxygen ions is considered to contribute most effectively to the hopping of the oxygen ions. Therefore, the frequency at 690 cm^{-1} in the spectra with T_{1u} symmetry may correspond to the attempt frequency.

In the cases of conductivity,[1-7] γ-γ angular correlation,[8] and quasielastic light scattering[9] measurements in this material, various values of the attempt frequency are reported. Our evaluated value of the attempt frequency is within the frequency range of the reported attempt frequencies. Generally, the experimentally evaluated attempt frequency depends on the experimental methods.[29] This may be due to the fact that the attempt frequency is a fitting parameter in many cases. However, the attempt frequency has a clear physical meaning in the defect-induced hyper-Raman spectra of cubic zirconia.

From the discussion above, the attempt frequency generally has frequency distributions. However, in cubic zirconia, the frequency distribution of the attempt frequency is separated into two frequency regions, as seen in Fig. 7: one is the isolated 690-cm^{-1} band and the other is the low-frequency region below 400 cm^{-1}. As the high-frequency part of these attempt frequencies will contribute mainly to the hopping rate of the ions, the hopping channel can be uniquely defined and the virtual attempt frequency can be determined as a single value without the frequency distribution. This is thought to be the main reason for the fact that, in the case of the measurements of hopping rates in other experimental methods, the attempt frequency can be determined as a single fitting parameter for cubic zirconia.

V. CONCLUSION

By using hyper-Raman scattering, vibrational properties of CaF_2 and cubic zirconia are investigated. For the CaF_2 crystal, the spectra show structures similar to the infrared absorption spectra, reflecting the similarity of selection rule for light matter interaction. In the case of cubic zirconia which has many vacancies, the defect-induced hyper-Raman spectra are found. These spectra are mainly elucidated by the frequency distribution of the defect-induced hyper-Raman-active modes in the whole Brillouin zone, which is calculated by using the defect space consisting of a vacancy and its nearest neighbor—six oxygen ions with symmetry O_h. From the analysis of mode vectors of the O_6 molecule, the attempt frequency for the oxygen-ion hopping is found to be included in the spectra of the hyper-Raman-active T_{1u} mode and the channel of hopping ions is uniquely defined for cubic zirconia giving the attempt frequency of 690 cm^{-1}.

ACKNOWLEDGMENTS

The authors are indebted to Mr. Y. Chiba for making the cubic zirconia crystals. The authors thank Professor H. Arashi for his useful discussions. This work is partly supported by a Grant-in-Aid for Special Project Research from The Ministry of Education, Science and Culture, Japan.

[1]J. M. Dixon, L. D. LaGrange, U. Merten, C. F. Miller, and J. T. Porter II, J. Electrochem. Soc. **110**, 276 (1963).
[2]D. W. Strickler and W. G. Carlson, J. Am. Ceram. Soc. **47**, 122 (1964).
[3]R. E. W. Casselton, Phys. Status Solidi A **2**, 571 (1971).
[4]A. I. Ioffe, D. S. Rutman, and S. V. Karpachov, Electrochim. Acta **23**, 141 (1978).
[5]P. Abelard and J. F. Baumard, Phys. Rev. B **26**, 1005 (1982).
[6]W. D. Kingery, J. Pappis, W. E. Doty, and D. C. Hill, J. Am. Ceram. Soc. **42**, 393 (1959).
[7]A. Nakamura and J. B. Wagner, Jr., J. Electrochem. Soc. **127**, 2325 (1980).
[8]A. Baudry, P. Boyer, and A. L. de Oliveira, J. Phys. Chem. Solids **43**, 871 (1982).
[9]T. Suemoto and M. Ishigame, Solid State Commun. **45**, 641 (1983).
[10]C. H. Perry and A. Feinberg, Solid State Commun. **36**, 519 (1980).
[11]T. Suemoto and M. Ishigame, Phys. Rev. B **33**, 2757 (1986).
[12]T. Suemoto and M. Ishigame, Solid State Ionics, **21**, 225 (1986).
[13]See, e.g., M. J. Delaney and S. Ushioda, in *Physics of Superionic Conductors*, edited by M. B. Salamon (Springer-Verlag, Berlin, 1979), p. 111.
[14]A. Feinberg and C. H. Perry, J. Phys. Chem. Solids **42**, 513 (1980).
[15]M. Ishigame and E. Yoshida, Solid State Ionics (to be published).

[16]M. Ishigame, E. Yoshida, S. Shin, and Y. Shimada, Solid State Ionics **20**, 105 (1986).
[17]See, e.g., H. Vogt, in *Light scattering in Solids II*, edited by M. Cardona and G. J. Güntherodt (Springer-Verlag, Berlin, 1982), p. 208.
[18]D. Michel, M. P. Jorba, and R. Collongues, J. Cryst. Growth **43**, 546 (1978).
[19]T. Sakurai, O. Kamada, K. Shishido, and K. Inagaki, Sol. Energy **8**, 117 (1964).
[20]H. Vogt and G. Neumann, Optics Commun. **19**, 108 (1976).
[21]H. Vogt and G. Neumann, Phys. Status Solidi B **92**, 57 (1979).
[22]H. Vogt and H. Presting, Phys. Rev. B **31**, 6731 (1985).
[23]P. Denham, G. R. Field, P. L. R. Morse, and G. R. Wilkinson, Proc. Soc. London, Ser. A **317**, 55 (1970).
[24]W. B. Lacina and P. S. Pershan, Phys. Rev. B **1**, 1765 (1970).
[25]D. Steele and B. E. F. Fender, J. Phys. C **7**, 1 (1974).
[26]S. J. Cyvin, J. E. Rauch, and J. C. Decious, J. Chem. Phys. **43**, 4083 (1965).
[27]K. Inoue, N. Asai, and T. Sameshima, J. Phys. Soc. Jpn. **50**, 1291 (1981).
[28]C. Pascual and P. Duran, J. Am. Ceram. Soc. **66**, 23 (1983).
[29]See, e.g., P. M. Richard, in *Physics of Superionic Conductors*, edited by M. B. Salamon (Springer-Verlag, Berlin, 1979), p. 162.